

Spreading out and staying sharp - Creating diverse rotation curves via baryonic and self-interaction effects

Peter Creasey^{1*}, Omid Sameie¹, Laura V. Sales¹, Hai-Bo Yu^{1†}, Mark Vogelsberger^{2‡} and Jesús Zavala³

¹ Department of Physics and Astronomy, University of California, Riverside, California 92507, USA

² Department of Physics, Kavli Institute for Astrophysics and Space Research, Massachusetts Institute of Technology, Cambridge, MA 02139, USA

³ Center for Astrophysics and Cosmology, Science Institute, University of Iceland, Dunhagi 5, 107 Reykjavik, Iceland

10 April 2017

ABSTRACT

Galactic rotation curves are a fundamental constraint for any cosmological model. We use controlled N-body simulations of galaxies to study the gravitational effect of baryons in a scenario with collisionless cold dark matter (CDM) versus one with a self-interacting dark matter (SIDM) component. In particular, we examine the inner profiles of the rotation curves in the velocity range $V_{\max} = [30 - 250]$ km s⁻¹, whose diversity has been found to be greater than predicted by the Λ CDM scenario. We find that the scatter in the observed rotation curves exceeds that predicted by dark matter only mass-concentration relations in either the CDM nor SIDM models. Allowing for realistic baryonic content and spatial distributions, however, helps create a large variety of rotation curve shapes; which is in better agreement with observations in the case of self-interactions due to the characteristic cored profiles being more accommodating to the slowly rising rotation curves than CDM. We find individual fits to model two of the most remarkable outliers of similar V_{\max} , UGC 5721 and IC 2574, the former a cusp-like rotation curve and the latter a seemingly 8 kpc cored profile. This diversity in SIDM arises as permutations of overly concentrated halos with compact baryonic distributions versus underdense halos with extended baryonic disks. The SIDM solution is promising and its feasibility ultimately depends on the sampling of the halo mass-concentration relation and its interplay with the baryonic profiles, emphasising the need for a better understanding of the frequency of extreme outliers present in current observational samples.

Key words: galaxies: formation - galaxies: evolution - galaxies: structure - cosmology: theory - methods: numerical

1 INTRODUCTION

Dark matter makes up 80% of the total mass budget in the Universe, but its exact nature remains doggedly elusive. Without direct detection of a single dark matter particle we have to infer its properties from its macroscopic distribution, and any observable that might hint at its underlying particulate nature is seized upon with vigour. A plethora of observations, such as large scale structures, lensing and scaling relations, and early fluctuations on the Cosmic Microwave Background, agree surprisingly well with predictions of a rather simple cosmological model with a cosmological constant, denoted as Λ , and a collisionless cold dark matter (CDM) component (e.g. Planck Collaboration et al. 2014). This Λ CDM paradigm has become the standard and most widely accepted model today for the observed Universe.

Λ CDM makes testable predictions at galactic scales that can be contrasted with observations. Among the most fundamental of them is for the structure of dark matter halos, with a density profile parameterised by a Navarro-Frenk-White (NFW) profile (Navarro et al. 1997), which at the inner radii scales as a power law $r^{-\alpha}$ with $\alpha \approx 1$. Observations, however, of the rotation curves of spiral galaxies, including dwarf and low surface brightness galaxies, often exhibit an inner circular velocity of stars and gas that increases more mildly than expected from a CDM halo (e.g. Flores & Primack 1994; Moore 1994; Persic et al. 1996; Kuzio de Naray et al. 2008; Oh et al. 2015), indicating an inner density profile shallower than the NFW cusp, i.e., $\alpha < 1$. This discrepancy can be further generalised as the mass deficit problem: the CDM halo contains too much dark matter mass in the inner regions than inferred from observations (Boylan-Kolchin et al. 2011; Ferrero et al. 2012; Papastergis et al. 2015; Papastergis & Shankar 2016; Schneider et al. 2016).

A more intriguing observation is that the galactic rotation curves exhibit a large diversity. Individual fits to galaxy rotation

* E-mail: peter.creasey@ucr.edu

† Hellman Fellow

‡ Alfred P. Sloan Fellow

curves span a spectrum from cores $\alpha \approx 0$ (e.g. Côté et al. 2000; de Blok et al. 2008; Kuzio de Naray et al. 2010) to cusps (e.g. van den Bosch et al. 2000; Swaters et al. 2003; Spekkens et al. 2005), and in the case of cored profiles, the central densities can differ by a factor of 10 for galaxies inhabiting similar halos (Kuzio de Naray et al. 2010). Recently, Oman et al. (2015) quantified this diversity in rotation curves by comparing $V_{2\text{ kpc}}$ for a fixed V_{max} , where $V_{2\text{ kpc}}$ is the circular velocity at 2 kpc and V_{max} is the peak circular velocity. For V_{max} in the range of 50–250 km s⁻¹, the scatter in $V_{2\text{ kpc}}$ is a factor of 3–4 and consequently the mechanism invoked to generate cored profiles must also accommodate this large variations in rotation curve shapes. Notably mass modelling is subject to significant uncertainties, especially at the scale of low mass dwarfs where pressure support effects, triaxiality, inclination, hidden bars and other irregularities hamper the utility of circular velocity profiles for mass modelling (Hayashi et al. 2004; Rhee et al. 2004; Pineda et al. 2017; Read et al. 2016b), making it hard to assess the precise spread in the rotation curves. In this paper, we take the result reported in Oman et al. as our reference.

The distribution of rotation curves is clearly too heterogeneous to be indexed with a single parameter. For example, several different galaxy formation models seem able to reproduce the Tully-Fisher (Tully & Fisher 1977) relation within Λ CDM (McCarthy et al. 2012; Brook et al. 2016; Di Cintio & Lelli 2016; Sales et al. 2017; Ferrero et al. 2017; Santos-Santos et al. 2016; Katz et al. 2017) provided the stellar feedback populates dark matter halos with the right stellar mass and size (though see also Pace 2016), yet despite this global consensus the circular velocity profiles predicted by each model differ in detail, with some cases leading to the formation of cores (e.g. Governato et al. 2010; Pontzen & Governato 2012; Di Cintio et al. 2014; Read et al. 2016a; Wetzel et al. 2016) whereas other simulations preserve the inner dark matter cusps (e.g. Sawala et al. 2015; Vogelsberger et al. 2014; Schaller et al. 2015). The disagreement may arise from the inclusion of different physical processes, different numerical implementation or may even vary with star formation histories (e.g. Oñorbe et al. 2015; Tollet et al. 2016).

In particular, the feedback model applied by Oman et al. (2015) appears unable to explain the scatter in observations within the Λ CDM framework. On the other hand, Brook (2015) finds good agreement between simulations and observations when looking at the scatter in the ratio between the circular velocity at 1 kpc and V_{max} . Similarly Read et al. (2016b) has also found consistency between baryon induced cores within Λ CDM and the shape of observed rotation curves. It is unclear, however, that this baryonic solution would hold if the size of the cores measured in observations is $\gtrsim 1$ kpc (see for instance Tollet et al. 2016). In fact, this may represent a serious limitation of this solution. For example IC 2574 has an inferred cored inner halo which extends for 8 kpc, well beyond the radius of the stars, with a stellar half-mass radius of 5 kpc. This type of object is a challenge to the hypothesis of feedback generated cores since, by construction, the extent of the cores in such scenarios is limited to the region where stars form and deposit their energy (Di Cintio et al. 2014).

An alternative solution is to consider cores formed out of self-interacting dark matter (SIDM), which we explore in this paper. The SIDM model retains important features of the CDM model including the distribution of halo concentrations as a function of mass (Rocha et al. 2013). SIDM differs, however, in that scattering between dark matter particles leads to heat transfer and the generation of dense cores in the inner regions of halos (Spergel & Steinhardt 2000; Firmani et al. 2000). Recent high-resolution N-body

simulations have shown that the self-interaction cross-section per unit mass $\sigma_{\text{T}}/m_{\chi} \sim 1 \text{ cm}^2 \text{ g}^{-1}$ is required to have core densities that are preferred by galaxy observations (Vogelsberger et al. 2012; Zavala et al. 2013; Rocha et al. 2013; Elbert et al. 2015). Kaplinghat et al. (2016) finds $\sigma_{\text{T}}/m_{\chi} \approx 1\text{--}3 \text{ cm}^2 \text{ g}^{-1}$ by directly fitting the rotation curves of dwarf galaxies. On the other hand, there are various constraints on $\sigma_{\text{T}}/m_{\chi}$, including merging clusters (Randall et al. 2008; Kahlhoefer et al. 2014; Robertson et al. 2017; Kim et al. 2016), shapes of elliptical galaxies and galaxy clusters (Miralda-Escudé 2002; Feng et al. 2010; Peter et al. 2013), core sizes of clusters (Yoshida et al. 2000; Rocha et al. 2013; Kaplinghat et al. 2016; Elbert et al. 2016), and survival of dwarf halos from evaporation (Gnedin & Ostriker 2001).

Among these constraints the strongest limit is $\sigma_{\text{T}}/m_{\chi} \lesssim 0.1 \text{ cm}^2 \text{ g}^{-1}$ in galaxy clusters (Yoshida et al. 2000; Kaplinghat et al. 2016; Elbert et al. 2016), where the relative dark matter velocity $v \sim 1500 \text{ km s}^{-1}$. As such, the self-interaction cross-section should have a mild velocity dependence, which can be naturally realised in a class of hidden sector dark matter models with a light force mediator (e.g. Feng et al. 2009, 2010; Buckley & Fox 2010; Loeb & Weiner 2011; Tulin et al. 2013a,b; Boddy et al. 2014, 2016). A velocity-dependent SIDM model, based a Yukawa potential, has been implemented in zoom-in N-body simulations (Vogelsberger et al. 2012, 2016), and further generalised in the ETHOS (Effective Theory of Structure Formation) framework, mapping underlying particle physics parameters to astrophysical observables (Vogelsberger et al. 2016; Cyr-Racine et al. 2016).

This approach has several distinct features that help explain the rotation curve diversity. Firstly, the scatter in the halo concentration leads to variations in core density directly (Kaplinghat et al. 2016). Secondly, the self-interactions thermalise the inner halo with its central dark matter density *dependent* upon the baryonic extent. In dark matter dominated galaxies, a dense core forms whose density is determined by the self-interaction cross-section and the halo mass. With a cored profile, the features in the baryon distribution are more prominently reflected in the rotation curves. In contrast, in galaxies where the baryon component dominates the potential, the thermalisation process lead to a denser central core with sizes influenced by the baryonic scale radius (Kaplinghat et al. 2014). Analytical calculations to address the diversity problem have been carried out by Kamada et al. (2016) using isothermal approximations to the effects of SIDM with a baryonic potential in order to construct fits for a diverse range of individual spiral galaxies.

In this work we explore the combined effects of SIDM and baryonic potentials by performing a series of numerical experiments. Our focus is on global trends but we include a pair of individual fits to test our results on the strongest outliers from observations. We sample a realistic range of concentrations and halo masses taken from cosmological simulations together with observed trends in the mass-size relation of galaxies. Our numerical approach and the analytical one presented in Kamada et al. (2016) complement each other in addressing the diversity problem in the SIDM model. The structure of this paper is as follows. In Section 2 we introduce in detail our simulations. Sections. 3.1 and 3.2 explore the diversity problem for a large sample of halos with $V_{\text{max}} = [30\text{--}250] \text{ km s}^{-1}$ with the latter including the effect of baryons. In Sec. 3.3 we confirm that we can find rotation curves that are reasonable matches to a pair of extreme (one cusp-like and one core-like) observed rotation curves. In Sec. 4 we summarise and conclude.

2 NUMERICAL SIMULATIONS

We use a combination of N-body simulations and analytical tools to study the mass profile of galaxies within the SIDM framework including the effects driven by their baryons. The main focus of this work is on disk dominated galaxies, which we model with a disk component embedded within a massive and more extended dark matter halo (i.e. no bulge). For the N-body simulations we must produce discretised initial conditions which we describe for the halo in Section 2.2 in addition to the baryonic potential in 2.3. We evolve these initial conditions with and without the effect of a baryonic disk and also with and without self-interaction terms using the simulation code described in Section 2.1.

2.1 N-body code

We use the AREPO code [Springel \(2010\)](#) with the modifications of [Vogelsberger et al. \(2012\)](#) and [Vogelsberger et al. \(2016\)](#) to account for dark matter self-interactions. This methodology uses a Monte-Carlo approach to model the scattering of dark matter via the probabilistic scattering of the macroscopic dark matter particles in the simulation, where the density distribution due to an individual particle is smoothed over some kernel which extends over the k -nearest neighbours. Such an explicit method requires a time step limit Δt_{sidm} such that only $\lesssim 1$ scattering can occur per particle per timestep. Notably in the cusp region of an NFW halo (i.e. $\rho \sim r^{-1}$ as $r \rightarrow 0$) as one moves towards the centre one finds that $\Delta t_{\text{sidm}} \propto \frac{1}{\rho\sigma} \sim r^{\frac{1}{2}}$ (with σ the velocity dispersion), i.e the centre of the halo is so dynamically cold and dense that the mean-free path is below the particle separation. To avoid such small time steps one additionally needs to limit them to a small fraction of the acceleration time step.

We have modified this code to include a baryonic potential of a Miyamoto-Nagai (hereafter MN) disk (Section 2.3) and used a constant self-interaction cross-section for scattering, which is a good approximation in the dark matter low velocity limit, e.g., $v \lesssim 400 \text{ km s}^{-1}$ as shown in Fig. 1 of [Kaplighat et al. \(2016\)](#).

In our calculations we assume a Hubble constant $H_0 = 70 \text{ km s}^{-1} \text{ Mpc}^{-1}$. Our simulation period is fixed at 10 Gyr, slightly shorter than the Hubble time ($H_0^{-1} \approx 13.96 \text{ Gyr}$) in order to account, in an approximate way, for the assembly time of such galactic disks. It should be emphasised that isolated simulations with a static disk potential is well-motivated in the SIDM model; for $\sigma_{\text{T}}/m_{\chi} \gtrsim 1 \text{ cm}^2/\text{g}$, dark matter self-interactions occur multiple times in the inner halo over the age of galaxies, which drive thermalisation of the inner halo in the presence of the stellar disk, and as such the final inner SIDM halo profile is more robust to changes in the formation history (given a known baryon distribution) than that of CDM.

2.2 Isolated halo initial conditions

For each of our galaxies, we generate a large set of compound galaxies consisting of an exponential disk embedded in a dark matter halo using the code MAKEDISK ([Hernquist 1993](#); [Springel et al. 2005](#)). The systems are set up in near equilibrium by requiring a joint solution to the combined phase space of both disk and halo component. In particular, the density profile of the halo is set up with a [Hernquist \(1990\)](#) density profile:

$$\rho_{\text{dm}}(r) = \frac{M_{\text{dm}} r_{\text{hq}}}{2\pi r (r + r_{\text{hq}})^3}, \quad (1)$$

with r_{hq} the scale radius of the halo. [Hernquist \(1990\)](#) profiles show a r^{-1} slope in the inner density profile and r^{-4} in the outskirts, in close agreement with the inner/outer slopes of -1 and -3 , respectively, of the cosmologically inspired NFW profiles ([Navarro et al. 1997](#)). The Hernquist profile has the extra advantage of having an analytic expression for its distribution function, which facilitates the process of setting up the initial conditions.

Hernquist halos can be “scaled” to match a given NFW profile quite closely and we therefore report our results in terms of virial mass¹ M_{200} and concentration parameter c corresponding to NFW halos. Finding the equivalent halo (by matching the dark matter mass within r_{200} and the asymptotic density profile as $r \rightarrow 0$) gives the relation between parameters

$$M_{\text{dm}} = M_{200} - M_{\text{d}} \quad (2)$$

$$r_{\text{hq}} = \left(\frac{GM_{200}}{100H_0^2} \right)^{1/3} c^{-1} \sqrt{2\ln(1+c) - \frac{2c}{1+c}} \quad (3)$$

dependent upon the baryonic component M_{d} and the redshift zero Hubble constant H_0 .

The matching of the internal regions of our Hernquist profile to the desired NFW is less accurate as we move close to the scale radius of the NFW r_{s} , with the density of a Hernquist halo falling off more steeply beyond that point. In terms of the velocity dispersion profile, the Hernquist halo has a peak velocity dispersion shell that is more compact and this velocity dispersion is lower than the NFW value. This can affect the heat exchange, which stops once the isothermal core has been established. As a consequence of the lower velocity dispersion peak, Hernquist profiles can be more prone to the so called “core collapse” phenomena, or the runaway collapse in the inner regions that ultimately reverses the process of mass scattering away from the core and condenses instead more mass in the inner regions. This process would be exacerbated by the presence of baryons and as $\sigma_{\text{T}}/m_{\chi}$ increases.

We have extensively tested this scenario and we include some comparisons in Appendix B. We find that it makes a negligible difference in most of our simulations except for extreme cases with concentrated halos, however as we shall see later it is the *low* concentration halos where most of the interesting discrepancy between CDM and SIDM predictions lie, i.e. these halos are expected to host the low central (dark matter) density galaxies that are most challenging to CDM. As such our approach of using Hernquist halos is conservative, as the effect will be small and any deviations will cause us to underestimate our conclusions.

For the simulations showed in Sec. 3, we set up our halos using $n_p = 10^5$ particles to model the dark matter distribution, which results in a spread for the mass per particle $m_p = 8.97 \times 10^4 - 2.66 \times 10^7 M_{\odot}$ according to the mass of the simulated halo. We use a gravitational softening length $\epsilon = 50 \text{ pc}$, and we have tested for numerical convergence using a halo with $M_{200} = 1.1 \times 10^{11} M_{\odot}$ and increasing/decreasing the particle number by a factor 10 with respect to our fiducial runs and find agreement within 10% in the (dark matter only) circular velocity profiles (and by proxy mass) for all radii outside 1.0 kpc.

2.3 Disk potential

The baryonic component of our galaxies is modelled by a fixed disk potential, which is not only computationally cheaper, but also

¹ Virial quantities are defined at the virial radius r_{200} , where the enclosed density is 200 times the critical density of the Universe.

allows us to maintain full control on the exact distribution of the baryons. This is particularly important for dwarf galaxies which undergo hundreds of orbits over a Hubble time and are thus particularly sensitive to (unphysical) discretisation-induced instabilities. We therefore strip the disk particles created in our initial conditions, and use instead an extra component in the gravitational force that accounts for the removed disk particles. This approach is not fully self-consistent since it ignores the back-reaction of the halo onto the baryons, but it provides a useful tool to explore the evolution of halo potentials in SIDM in a set of controlled experiments where the *final* baryonic distribution is known.

We implemented a static potential in AREPO following a Miyamoto & Nagai (1975) disk:

$$\Phi_{\text{MN}}(R, z) = \frac{-GM_{\text{d}}}{\sqrt{R^2 + (R_{\text{d}} + \sqrt{z_{\text{d}}^2 + z^2})^2}}, \quad (4)$$

for a disk of mass M_{d} and scale radius R_{d} and we keep the disk relatively thick in all cases by setting $z_{\text{d}}/R_{\text{d}} = 0.3$ (appropriate to model dwarf irregular galaxies). Note that the half-mass radius of the flat ($z_{\text{d}} = 0$) MN disk is $\sqrt{3}R_{\text{d}}$ which is very close to the ratio of half-mass to scale radius of an exponential disk of 1.678 and so unless ones disk is extremely thick, the scale radius of an exponential fit will be within a few percent². From here on we will use R_{d} interchangeably to refer to either the scale length of our baryonic disks in simulations (the MN scale radius) or the exponential disks associated with observed late-type dwarf galaxies.

Notice that the initial conditions are created assuming an exponential profile while the fixed potential uses an MN model for the disk. We have tested that this small inconsistency does not affect our results. Due to the diffusive nature of SIDM the resulting deviations due to non-equilibria are of the order of a few percent and quickly damped. Alternative approaches include that of Elbert et al. (2016) where the MN disk is ‘grown’ adiabatically (compared to the orbital timescale) from an initially halo-only setup. We have tested the extreme case of inserting the fixed potential instantaneously and find that after 10 Gyr evolution in SIDM at 2 kpc this makes a relative difference in the $V_{2 \text{ kpc}}$ of -0.2 km s^{-1} or 0.6%. Our method, being closer to equilibrium, is expected to be lower than these bounds.

We run the simulations for 10 Gyr and compute the circular velocity profiles. For the CDM cases this is in the most part a straightforward numerical test since the initial conditions are created in equilibrium and we do not see significant evolution of the mass distribution with time. For the most extended disks ($R_{\text{d}} = 6 \text{ kpc}$), however, the centre-of-mass is not well ‘tied’ to the centre of the (shallow) baryonic potential, and the centre-of-mass can ‘drift’ on the order of a kpc over 10 Gyr (i.e. an average of 0.1 km s^{-1}) from the centre of the baryonic disk potential, making the assessment of the mass distribution within 2 kpc problematic. This evolution is expected due to discretisation of ICs and asymmetry in tree-based gravitational methods, and is relatively hard to suppress even with a tight timestep criteria. This process can of course also occur to the SIDM halos, although it is somewhat suppressed since their profiles have less compact centres. Since evolving CDM halos in extreme cases is somewhat tangential to the purpose of this paper, however, we have tested the CDM evolution on

² The differences are much more pronounced in the tails of the distribution, indeed one cannot choose to correspond a flat exponential to a MN density profile via for example the mass weighted root-mean square radii since for the latter that is a divergent quantity.

the more compact ($R_{\text{d}} = 0.5$ and 1.5 kpc) halos, whose $V_{2 \text{ kpc}}$ evolve by an average of -7.7% over 10 Gyr. For the $R_{\text{d}} = 6 \text{ kpc}$ CDM halos we will use the initial conditions, as we believe those to be more accurate.

3 RESULTS

3.1 Circular velocity profiles in dark matter only halos

To illustrate the effect of dark matter self-interactions on the density profile of a dwarf halo without the influence of baryons, we use the analytical Jeans method proposed in (Kaplinghat et al. 2014, 2016) and tested against simulations in (Rocha et al. 2013; Elbert et al. 2015). We have further checked that its accuracy is within 10–20% compared to the results from our N-body code (Vogelsberger et al. 2012). The details of the formalism can be found in Appendix A.

Our suite of halos aims to span the ‘dwarf’ galaxy distribution with 7 halos of V_{200} from 15–200 km s^{-1} , the upper limit being near Milky Way-like (where velocity dependent corrections may play some role) down to dwarfs so baryon-poor that we expect negligible deviations from the DM-only results. To encompass the diversity in concentrations we sample $\pm 2\sigma$ deviations from the cosmological mass-concentration relation presented in Ludlow et al. (2014), whose median is well approximated by the linear fit

$$c = 10.51 \times \left(\frac{M_{200}}{10^{11} \text{ M}_{\odot}} \right)^{-0.088}, \quad (5)$$

and at each halo mass the distribution is approximately log-normal where 1σ corresponds to a ratio of ≈ 1.25 . The corresponding halo mass (M_{200}) and NFW r_s and ρ_s are given for the $70 \text{ km s}^{-1} \text{ Mpc}^{-1}$ cosmology in Table 1.

The left panel of Fig. 1 shows the density profiles of a halo with $V_{200} = 70 \text{ km s}^{-1}$ ($M_{200} = 1.1 \times 10^{11} \text{ M}_{\odot}$) and a concentration $c = 6.65$ after 10 Gyr evolution with CDM ($\sigma_{\text{T}}/m_{\chi} = 0 \text{ cm}^2 \text{ g}^{-1}$, black dashed line) vs. SIDM with $\sigma_{\text{T}}/m_{\chi} = 2, 5$ and $10 \text{ cm}^2 \text{ g}^{-1}$ (see solid lines according to labels). The radius of unit scattering, r_1 (see also Appendix A) outside of which the halo is undisturbed is marked for the three cases. This radius grows with cross-section, and in the interior we see all three cross-sections produce cores for this halo that extend beyond 2 kpc.

Fig. 1 (right panel) shows the circular velocity of the SIDM halo profiles evaluated at 2 kpc as a function of V_{max} . For the comparison, we also plot the corresponding CDM one with the mass-concentration relation from Ludlow et al. (2014) and the range spanned by a compilation of the observed rotation curves in galaxies taken from Oman et al. (2015). It is clear that $V_{2 \text{ kpc}}$ increases steadily with V_{max} in the case with CDM, although the relation stays below the 1 : 1 line. In contrast, SIDM predicts a much shallower relation. $V_{2 \text{ kpc}}$ is almost independent of V_{max} in the range explored, and the median $V_{2 \text{ kpc}}$ value at a given V_{max} depends mildly on cross-section. For low mass halos (low circular velocity), V_{max} tends to converge to near $V_{2 \text{ kpc}}$, since the objects are small and the core size becomes much less than 2 kpc and V_{max} is measured near 2 kpc. It is interesting to note this is a common feature in CDM as well as SIDM halos. Shaded regions indicate $\pm 1\sigma$ in concentration (we interpolate from the $\pm 2\sigma$).

The range of $V_{2 \text{ kpc}}$ and V_{max} statistics of the galaxy rotation curve distribution is shown in Fig. 1 (taken from Oman et al. 2015). The scatter found in the data is significantly larger than derived purely from that of concentration variations (in either CDM or SIDM). A large fraction of the observed $V_{2 \text{ kpc}}$ scatter below the relation expected for CDM, suggesting that such objects have

V_{200} (km s ⁻¹)	M_{200} (M _⊙)	concentration (-2σ, median, +2σ)	r_s (kpc) -2σ, med., +2σ	ρ_s (10 ⁶ M _⊙ kpc ⁻³)* -2σ, med., +2σ	M_d (M _⊙)	med. R_d (kpc ^{**})
15	1.12×10^9	9.99, 15.60, 24.38	2.15, 1.37, 0.88	6.07, 18.42, 57.80	†	†
30	8.97×10^9	8.32, 12.99, 20.30	5.15, 3.30, 2.11	3.89, 11.63, 36.04	1.71×10^8	(1.93)
50	4.15×10^{10}	7.27, 11.36, 17.74	9.83, 6.29, 4.03	2.82, 8.32, 25.52	8.84×10^8	(2.53)
70	1.14×10^{11}	6.65, 10.39, 16.23	15.04, 9.62, 6.16	2.29, 6.69, 20.36	2.79×10^9	(3.03)
100	3.32×10^{11}	6.05, 9.46, 14.78	23.60, 15.11, 9.67	1.84, 5.31, 16.05	1.09×10^{10}	(3.60)
150	1.12×10^{12}	5.44, 8.50, 13.28	39.41, 25.22, 16.14	1.43, 4.10, 12.27	3.72×10^{10}	(4.09)
200	2.66×10^{12}	5.04, 7.88, 12.30	56.69, 36.28, 23.22	1.20, 3.42, 10.15	6.22×10^{10}	(4.53)

Table 1. Parameters for the halos used in our diversity analysis. V_{200} and M_{200} , concentrations with $\pm 2\sigma$ relative to the median relation from Ludlow et al. (2014), and in NFW parameters we give the scale radius r_s and density ρ_s for this range of concentrations. For the simulations where we include a baryonic disk, M_d refers to the total baryonic disk mass.

* NFW density ρ_s is computed in the dark matter-only halo case. For the simulations with baryonic disks we fix M_{200} but add a baryonic component, and thus ρ_s is multiplied by the dark fraction M_{dm}/M_{200} .

** We quote median baryonic disk radii only for reference, since we attempt to span the distribution with 0.5-6 kpc as described in the main text.

† This halo was simulated in DM-only.

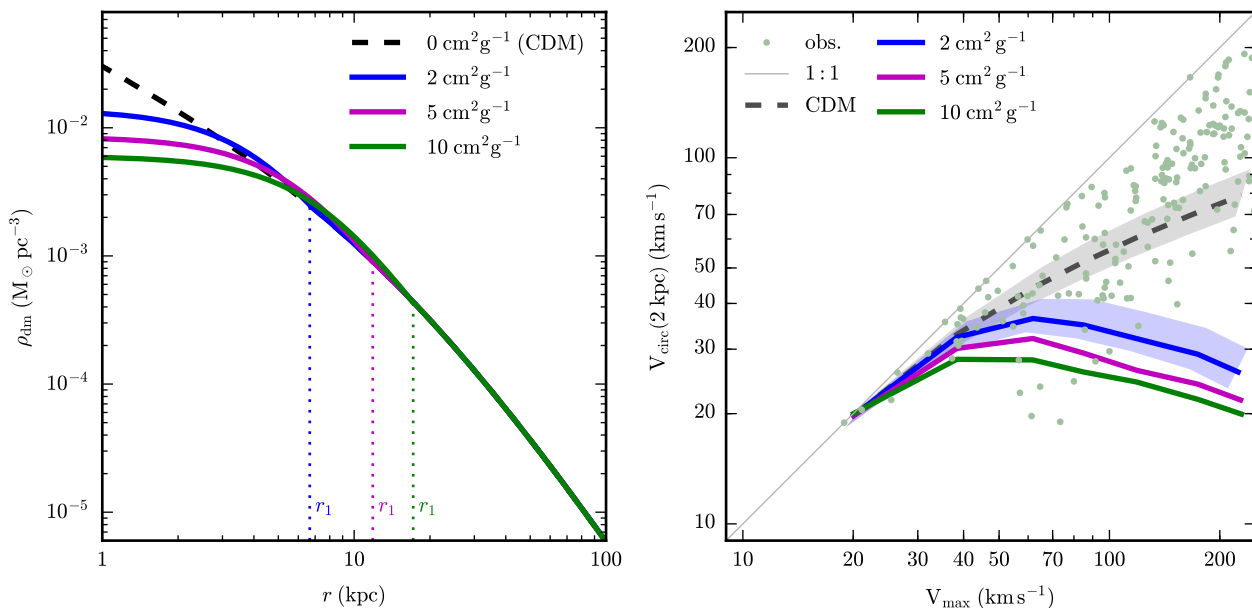


Figure 1. *Left panel:* core formation in a dark matter only halo (NFW) with different σ_T/m_χ . Dark matter density profile evolution for SIDM over 10 Gyr in blue, magenta and green for $\sigma_T/m_\chi = 2, 5$ and $10 \text{ cm}^2 \text{ g}^{-1}$ respectively, with CDM ($\sigma_T/m_\chi = 0 \text{ cm}^2 \text{ g}^{-1}$) in black dashed. Vertical dotted lines indicate r_1 (the radius of unit scattering). *Right panel:* effects of SIDM on the $V_{2 \text{ kpc}}$ vs V_{max} relation compared to CDM for dark matter only halos. Black line is the CDM case, blue the $\sigma_T/m_\chi = 2 \text{ cm}^2 \text{ g}^{-1}$ where the shaded regions denote $\pm 1 \sigma$ scatter (due to halo concentrations; we have interpolated the values from the $\pm 2\sigma$ runs in Table 1). Magenta and green denote $\sigma_T/m_\chi = 5 \text{ cm}^2 \text{ g}^{-1}$ and $10 \text{ cm}^2 \text{ g}^{-1}$ respectively. Green points indicate observed values collated in Oman et al. (2015) Table 1, from which we also include the mass deficits, 5×10^8 and $10^9 M_\odot$ and their effect on $V_{2 \text{ kpc}}$ in blue shaded regions.

a lower dark matter density in the inner regions than predicted by the model. Instead, self-interactions seem to have the opposite behaviour, providing a better match to these low density objects but predicting too low a $V_{2 \text{ kpc}}$ to explain most of the data. These calculations, however, ignore the contribution of the baryons, and as we argue below, the mass and radial extent of the gas and stars in galaxies may significantly change this prediction to bring SIDM in closer agreement with observations.

3.2 Circular velocity profiles in the presence of baryons

For collisionless dark matter halos, the presence of baryons may change the shape of the *total* circular velocity profile by adding

the contribution from the gas and the stars. This contribution may or may not change the overall profile, depending on the relative fraction of baryonic mass and also the spatial distribution of these baryons³. If gas and stars are very centrally concentrated, they will dominate the contribution to the circular velocity modifying the profile to rise more steeply than the original NFW halo. On the other hand, if the baryons are fairly extended, their contribution could be sub-dominant to the dark matter, in which case the to-

³ Notice that baryons could additionally cause the dark halo to contract (Blumenthal et al. 1986), but given our initial condition set-up, the halos will be created already in equilibrium with the baryonic potential

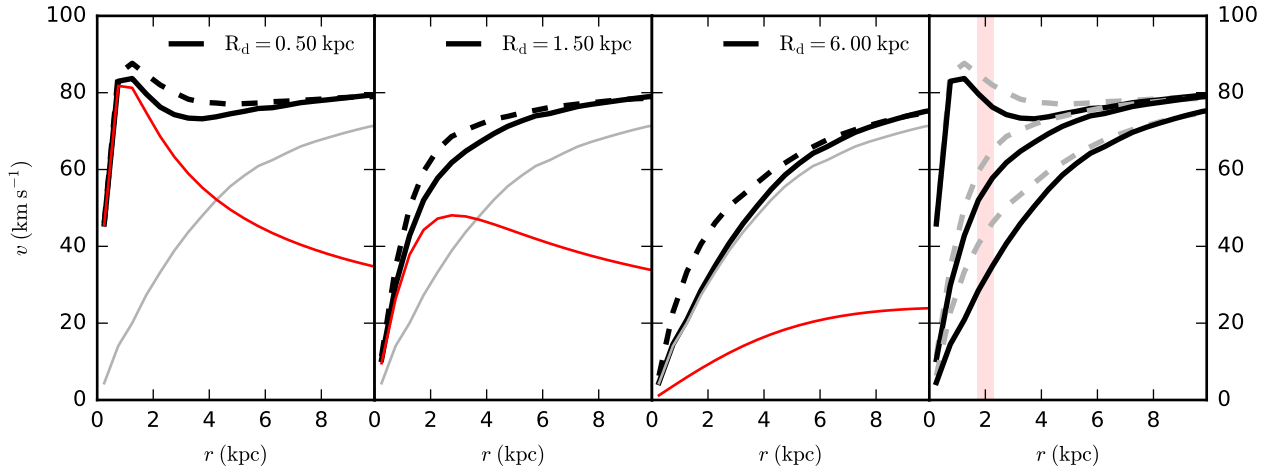


Figure 2. *Left three panels:* Dark matter contribution to the circular velocity profile for a dwarf galaxy ($V_{200} = 70 \text{ km s}^{-1}$, $c = -2\sigma$) with a fixed baryonic disk component with scale radii 0.5, 1.5 and 6 kpc from left to right respectively, simulated for 10 Gyr with a cross-section $\sigma_T/m_\chi = 2 \text{ cm}^2 \text{ g}^{-1}$. *Red lines* indicate the baryonic contribution, *grey* the dark matter (SIDM), and *thick solid black* the total. For comparison, the *thick dashed black* lines indicate the CDM total. *Right panel* combines the three profiles, with the CDM comparisons in *grey dashed* lines.

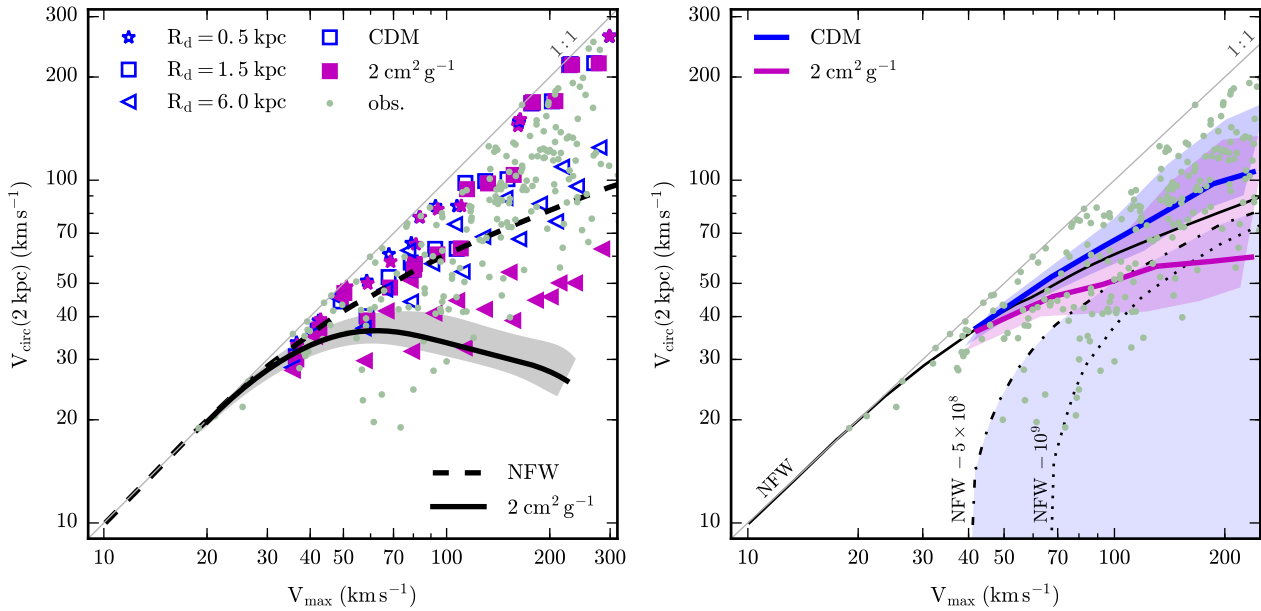


Figure 3. N-body simulations in the presence of galactic disks. *Left panel* shows the individual simulations with disk scale lengths $R_d = 0.5, 1.5$ and 6 kpc in *stars, squares and triangles* respectively, where each is repeated for the three different -2σ , median, and $+2\sigma$ concentrations and SIDM in *solid magenta* and CDM in *open blue symbols*. *Dashed black line* indicates the CDM relation without baryons, and *solid black* the corresponding SIDM (with $\pm 1\sigma$ shading). *Right panel* shows $2\text{-}\sigma$ likelihood contours about the median R_d and concentration (*solid lines*) for CDM in the presence of a baryonic disk in *blue* and SIDM in *magenta*, inferred from the fits in Eqns. (7) and (8), (see also main text). *Green points* indicate observed values collated in Oman 2015 Table 1.

tal velocity profile including baryons does not deviate significantly from that of the original NFW halo.

Fig. 2 (leftmost three panels) illustrates this point using the N-body simulations set up described in Sec. 2. For a fixed halo with $V_{200} = 70 \text{ km s}^{-1}$, $M_d = 2.8 \times 10^9 M_\odot$ (according to abundance matching relations from Behroozi et al. (2013)) and a concentration -2σ below the median. We plot the equivalent ‘circular velocity’ inferred for a spherically averaged mass distribution

$$V_{\text{cir}}^2 = GM(r)/r = V_{\text{cir,dm}}^2 + V_{\text{cir,bar}}^2 \quad (6)$$

which is an approximation for non-spherical distributions (for a

pure thin MN disk without a halo these deviations are at maximum $\approx 15\%$). We assume that the baryons distribute in a MN disk with scale length equivalent $R_d = 0.5, 1.5$ and 6 kpc (left to right). The long-dashed lines indicate the final profiles including the baryons for CDM, which show different shapes according to R_d , with the differences tracing back to the contribution of the baryons in each case.

As expected, a more concentrated baryonic distribution (small R_d) shows a steep raise of the circular velocity curve, whereas larger R_d values grow more gently. The case with $R_d = 0.5 \text{ kpc}$ re-

sults in a declining circular velocity profile which might not be the typical galaxy included in studies of rotation curves (probably representing a bulge dominated object instead). However, we include this case for illustration of the possible extremes and how CDM and SIDM would react to the presence of such a compact galaxy.

The same exercise of considering a fixed halo and baryonic content but changing the spatial distribution can be done assuming the SIDM scenario. The three left panels in Fig. 2 show the expected total profiles assuming a self-interaction cross-section $\sigma_T/m_\chi = 2 \text{ cm}^2 \text{ g}^{-1}$ (see solid black lines). The dark matter component still shows a cored profile due to the self-interactions (see thin grey line) but this is obscured in the *total* velocity profile. In fact, the inclusion of baryons creates a fair amount of *diversity* in the shapes of the circular velocity profiles for CDM and SIDM (see right panel in the same figure). For example, if we measure $V_{2 \text{ kpc}}$ in these halos (vertical red shaded region), CDM covers a range $\approx 45 - 83 \text{ km s}^{-1}$ which is comparable to that spanned by SIDM, $V_{2 \text{ kpc}} \approx 30 - 75 \text{ km s}^{-1}$. Encouragingly, the effect of baryons in the case with self-interactions creates a wide range of (total) rotation curves but also maintains a lower central density (in the cases where baryons are extended), allowing better accommodation of the low $V_{2 \text{ kpc}}$ values that are occur in observations (see right panel Fig. 1) and for which CDM alone has no explanation.

We generalise this by simulating all halos introduced in Sec. 3.1 but including a baryonic disk. The mass of the disk is the sum of a stellar and gaseous component, with the first set by the abundance matching relation between M_* and M_{200} introduced in Behroozi et al. (2013) and the gas mass computed from the $M_{\text{gas}}-M_*$ relations of Huang et al. (2012). To account for variations in halo concentration c , we sample three different halos of median and $\pm 2\sigma$ extremes according to the mass-concentration relation from Ludlow et al. (2014). Table 1 summarises the main properties of all our runs. Each halo is then set up in equilibrium with their baryonic MN disk of scale lengths $R_d = 0.5, 1.5,$ and 6.0 kpc . We fix the scale height of the disks to $z_d = 0.3R_d$, a slightly hotter structure than for Milky-Way-like galaxies but that provides a reasonable description of lower mass galaxies, the main target of this study.

We run our simulations for 10 Gyr assuming *i*) collisionless cold dark matter (CDM) and *ii*) a fiducial self-interaction cross-section $\sigma_T/m_\chi = 2 \text{ cm}^2 \text{ g}^{-1}$ for the SIDM case. We investigate the relation between V_{max} and $V_{2 \text{ kpc}}$ of our halos in CDM and SIDM in the left panel of Fig. 3. Symbol shapes (square, star, triangle) indicate the different scale lengths sampled whereas open-blue and filled-magenta differentiate between CDM and SIDM runs. A quick inspection suggests that self-interactions are able to generate a wider range of $V_{2 \text{ kpc}}$ at fixed V_{max} which is in better agreement with observed values from the compilation in Oman et al. (2015) (green dots). The diversity in both cases, CDM and SIDM, arises from different contribution by the baryons. Since SIDM cores imply a lower dark matter density in the inner regions, the contribution of baryons is *more* important than in the collisionless case, creating a larger variety in $V_{2 \text{ kpc}}$. Notice that for the more compact disks ($R_d = 0.5$ and 1.5 kpc) the predictions from CDM and SIDM are not that different, and in both cases $V_{2 \text{ kpc}}$ can be very close to V_{max} , which suggests these rotation curves are relatively flat. One should also note that in a cosmological context the central density would be even further promoted by the adiabatic contraction introduced by baryonic collapse (e.g. Elbert et al. 2016), which occurs even in the models with bursty feedback (Tollet et al. 2016). In the case with non-dominant baryonic components (triangles) the points stay close to the dark matter-only case (thin solid lines), which is

significantly lower in the case of self-interactions, as discussed in Sec. 3.1.

The lower envelope of points in either scenario corresponds to the most extended disks populating the -2σ outliers in halo concentration. A few of the observed points in the left panel of Fig. 3 still remain unexplained ($V_{\text{max}} \approx 70 \text{ km s}^{-1}$ and $V_{2 \text{ kpc}} \approx 20 \text{ km s}^{-1}$) showing central densities even lower than can be obtained in SIDM with $\sigma_T/m_\chi = 2 \text{ cm}^2 \text{ g}^{-1}$. This could be suggesting the need for a larger cross section for self-interactions or more extreme outliers on the mass-concentration relation. We should also bear in mind the possibility of observational errors as discussed in Sec. 1.

Although the exercise of fixing R_d is more clear and intuitive, in practise we know that galaxy size will scale with stellar mass, and the average behaviour in $V_{\text{max}}-V_{2 \text{ kpc}}$ plane will depend on the average R_d of the population at fixed V_{max} . In the right panel of Fig. 3 we take this into account as follows. The first step is to characterise R_d as a function of V_{max} . Because of the tight relation between halo mass and stellar mass, this is equivalent to finding a relation between R_d and M_* or, in our case, M_d . We compute the stellar size of the disk and then estimate the baryonic one by a simple correction by gas fraction. In detail, for our stellar radii we use a fit to the late-type SDSS galaxies of Shen et al. (2003):

$$R_* = 0.1 \left(\frac{M_*}{1 M_\odot} \right)^{0.14} \left(1 + \frac{M_*}{3.98 \times 10^{10} M_\odot} \right)^{0.25} \text{ kpc} \quad (7)$$

with scatter

$$\sigma_{\ln R} = 0.34 + \frac{0.13}{1 + \left(\frac{M_*}{3.98 \times 10^{10} M_\odot} \right)^2} \quad (8)$$

along with an estimate of the baryonic size as: $R_d = (1 + f_{\text{gas}})R_*$, where f_{bar} is estimated from M_* and observations by Huang et al. (2012) as explained before. This procedure then provides a median and $\pm 2\sigma$ disk radii for each halo mass. We then take these dispersions in R_d and interpolate between our simulations to find the appropriate V_{max} and $V_{2 \text{ kpc}}$, finally combining this dispersion in quadrature with the dispersion due to the M_{200} -concentration relation to infer the median and $\pm 2\sigma$ likelihood regions as a function of halo mass.

These likelihood regions are shown in the right panel of Fig. 3. The expected median in each scenario is notably shallower than the points in the left panel, which is mainly due to the average disk size rising as V_{max} increases. Indeed, as we saw in the left panel of the same figure, at fixed V_{max} a more extended baryonic disk will have lower $V_{2 \text{ kpc}}$. For comparison we include the effects of the mass deficits of 5×10^8 and $10^9 M_\odot$ within 2 kpc. Several observed points still scatter above and below the median relations for both CDM and SIDM hinting at the need of more extreme outliers (more than 2σ) to explain such objects.

We have probably overstated the extremity of these outliers since we have at zero-th order ignored correlations between halo and disk properties that would alleviate the tension. For instance, if more compact disks systematically populate more concentrated halos whereas extended disks live in low concentration halos, the shaded areas could be larger. We have also not made an attempt to account for observational biases in these calculations. Regardless of the absolute value, however, we emphasise that at fixed assumptions, SIDM seems to always provide a larger range of diversity than CDM (with scatter at least 150% of the latter).

An interesting corollary of the analysis above is that, fixing the relation $V_{\text{max}}-V_{2 \text{ kpc}}$, a given halo in CDM and SIDM would be

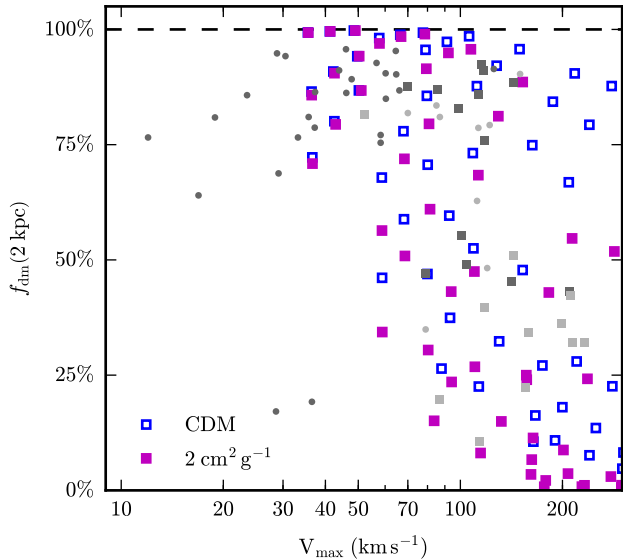


Figure 4. Dark matter contribution to the rotation curve at 2 kpc for SIDM simulations and observed dwarfs (see main text). *Filled magenta squares* are the SIDM simulations, in comparison to the CDM in *open blue squares*. *Greyscale symbols* refer to observed galaxies from (Oh et al. 2015) (*dark circles*), Kuzio de Naray et al. (2008) (*light circles*), de Blok et al. (2001) (*light squares*) and de Blok et al. (2008) (*dark squares*).

predicted to have different contribution from the baryons at 2 kpc, since in SIDM the baryonic matter will have to “compensate” for the lower density of the cored dark matter halo. It is therefore important to compare the dark matter fractions predicted in both models to check that they are consistent with observed galaxies. Fig. 4 shows the dark matter fractions $f_{\text{dm}} = M_{\text{dm}}/M_{\text{tot}}$ measured at 2 kpc for our CDM and SIDM halos (open and filled symbols, respectively) compared to a subsample of galaxies taken from the rotation curves presented in (Oh et al. 2015) and Kuzio de Naray et al. (2008). For the former we use their disk-halo decomposition from the stellar, HI and kinematic data, and for Kuzio de Naray et al. (2008) we use their ‘popsynth’ mass modelling rather than the extremal fits. In a couple of cases the last-measured point does not reach 2 kpc and for these we used the dark matter fraction at the last measured point.

There is a significant overlap between the collisionless and the self-interacting scenarios. Also, spatial resolution coupled to uncertainties in the mass-to-light ratios for the observed objects makes f_{dm} probably not a good enough indicator to distinguish between these alternative models. Nonetheless, it is reassuring that the same SIDM objects that reproduce better the observations in the $V_{\text{max}}-V_{2 \text{ kpc}}$ plane, seem to have dark matter fractions that are consistent with current observations.

3.3 Two extreme examples: IC 2574 and UGC 5721

In Sec. 3.2, we presented a detailed statistical analysis of a sample of objects simulated within the SIDM paradigm. This, however, left unexplained one of the main motivations of this work, which is the existence of extreme outliers which are not possible to accommodate within the standard CDM scenario. We turn then our attention to two particular examples highlighted in Oman et al. (2015), UGC 5721 and IC 2574. These two galaxies have similar circular velocity measured at the outermost point of the rotation

Property	Symbol	IC 2574	UGC 5721
Disk scale length	R_d	3.0	0.50 kpc
Disk scale height	z_d	0.9	0.15 kpc
Stellar mass	M_*	3.00×10^8	$4.48 \times 10^8 M_\odot$
Gas mass [†]	M_{gas}	2.72×10^9	$8.47 \times 10^8 M_\odot$
Halo mass	M_{200}	9.78×10^{10}	$5.15 \times 10^{10} M_\odot$
Concentration	c	6.2 (-2.3σ)	13.6 ($+0.9\sigma$)
DM cross-section	σ_T/m_χ	3	$3 \text{ cm}^2 \text{ g}^{-1}$
NFW radius	r_s	15.4	5.65 kpc
NFW density	ρ_s	1.9×10^{-3}	$0.013 M_\odot \text{ pc}^{-3}$

Table 2. Parameters for the SIDM halos and baryonic potentials for the two galaxies in Fig. 5 and 6.

[†] The gaseous component as added in post-processing due to its disturbed nature, see also main text in Sec. 3.3.

curve $\approx 80 \text{ km s}^{-1}$, which probably indicate that they populate dark matter halos with similar mass, but the *shapes* of the inner regions are remarkably different: whereas UGC 5721 is consistent with a ‘cuspy’ NFW profile, IC 2574 has a very extended core. This pair is an interesting case of the aforementioned diversity and we can use it as benchmark for our SIDM scenario.

In Figs. 5 and 6 we show the data together with the best fit CDM (dashed line) and SIDM (solid black) curves. For UGC 5721 (NGC3724) we use the rotation curve data from Swaters et al. (2003) and stellar and gas densities from Andrew Pace (priv. communication, for comparison one can see Fig. 1 in Swaters et al. 2010 which has a slightly higher mass-to-light ratio).

For IC 2574 we use the rotation curve, gas and stellar densities from Oh et al. (2011). We multiply the stellar velocity contribution by 0.5 (mass-to-light ratio lower by a factor 4), so the stellar contribution lies between that in Sanders & McGaugh (2002) and Oh et al. (2011). For both cases our SIDM halo is run using a cross section for self-interactions of $\sigma_T/m_\chi = 3 \text{ cm}^2 \text{ g}^{-1}$ following Kamada et al. (2016).

Our fitting process relied upon making an initial guess for the halo mass using V_{max} and sampling the concentration with $\pm 2.5\sigma$ of the mass-concentration relation in Eqn. (5). The combined stellar plus gaseous disks in these dwarfs are not well represented by a single MN disk (especially their gas profiles which exhibit a much more extended, nearly constant surface density), however since these differences are primarily in the outer regions where we expect the effects of self-interactions to be sub-dominant, we chose to approximate only the *stellar* distribution with an MN disk and apply the gas contribution to the rotation curve in a post-processing step (i.e. add in quadrature as in Eqn. 6), and after several iterations with the disk component we find the parameters indicated in Table 2. As noted in Appendix B, the initial conditions are constructed with Hernquist profiles converted from the corresponding NFW parameters, but if one is using a real NFW then in the higher concentration case using a lower r_s would give a slightly better match.

Fig. 5 shows that the SIDM fit for UGC 5721 including all components has an overall “cuspy” profile (see black solid line), which is *steeper* than the circular velocity expected for the corresponding NFW halo without self-interactions (dashed line). For this fit we need a concentrated halo at $+1\sigma$ above the median mass-concentration relation, which together with the observed compact stellar disk (scale radius of 0.5 kpc) combine to create a steeply raising velocity curve. This is an excellent example of the im-

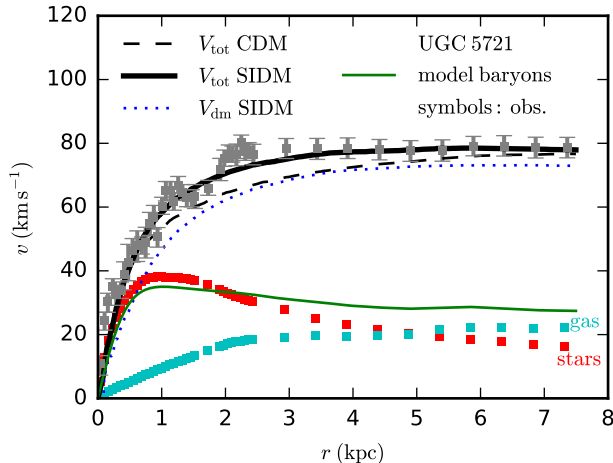


Figure 5. Observations for UGC 5721 along with SIDM and CDM simulations. Red points indicate the stellar contribution, cyan the gas and grey squares with error bars the observed rotation curve. The SIDM simulation (with parameters from Table 2) has the baryonic mass contribution indicated by the green line, which is a composition of the interpolated gas distribution along with an MN fit to the stellar disk. The halo contribution is given in the dotted blue line and the total curve in solid black. The comparison curve for CDM is given in the dashed black line.

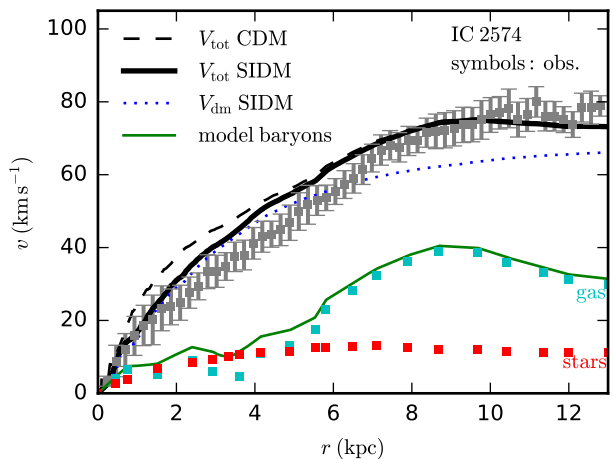


Figure 6. Observations for IC 2574 along with SIDM and CDM simulations. Red points indicate the stellar contribution, cyan the gas and grey squares with error bars the observed rotation curve. The SIDM simulation (with parameters from Table 2) has the baryonic mass contribution indicated by the green line, which is a composition of the interpolated gas distribution along with an MN fit to the stellar disk. The halo contribution is given in the dotted blue line and the total curve in solid black. The comparison curve for CDM is given in the dashed black line.

portance of baryons in the shape of the rotation curves, even for dwarf galaxies. The χ^2/dof of the SIDM fit is 3.04 (4.44 below the initial, which is of course not the best individual CDM halo fit). The visual impression of a superior fit is likely due to This χ^2 is largely driven by the $\lesssim 0.3$ kpc data with tight error bars over a non-monotonic feature, contributing to a visually impression of a superior fit. Clearly a more accurate fit to such features would require additional parameters (particularly for the stellar components), however this is outside the scope of this paper. Without the presence of baryons, UGC 5721 is a challenge for SIDM due to

the development of an extended low density core at the centre. In our simulations, however, the SIDM thermal transfer in cooperation with the baryon dominance in the central 1.5 kpc causes the halo to shrink even further than the pure NFW model. The compact stellar component excavates a potential well sufficient that thermalisation of the dark component leads to an almost-NFW final configuration (see also Kamada et al. 2016).

On the other hand, Fig. 6 presents the rotation curve fit for IC 2574 with an extended and slowly rising core in its centre. The gas has a disturbed profile, but the baryons as a whole contribute little to the total density except within the innermost 0.5 kpc, and make a modest contribution at $r > 6$ kpc. For such a dark matter dominated galaxy to deviate so far from a cusp-like profile is clearly a challenge for vanilla CDM (Blais-Ouellette et al. 2001; Sanders & McGaugh 2002; Swaters et al. 2003, 2010). Notice that any baryonic solution to this problem within CDM – for instance assuming that supernova feedback can create a core – would not work for such object, since the core extends well beyond where the stars are (see discussion in Oman et al. 2015). The χ^2/dof of the SIDM fit is 1.57, (1.39 below the initial conditions), which reflects the introduction of the core and quantifies the capacity of SIDM as a solution to this conundrum.

Whilst SIDM is relatively efficient in producing cores, this process becomes increasingly sedate as the core size approaches the scale radius of the halo (in this case 15.4 kpc) and so we have had to choose a relatively large scale radius (i.e. low concentration) halo. The $V_{2\text{ kpc}}$ of our CDM halo is around 35 km s^{-1} whilst in SIDM it is around 27 km s^{-1} , bringing it in better agreement with the observed rotation curve $V_{2\text{ kpc}} \approx 23\text{ km s}^{-1}$.

We note that for IC 2574 both the low concentration and self-interactions are required to achieve a good fit. As such one way to test our model is to perform a statistical study of extreme outliers like IC 2574. Since we assume the SIDM model inherits the halo mass-concentration relation of the CDM one, such a study also provides a direct test for ΛCDM on galactic scales.

We have shown that the SIDM model in the presence of baryons can provide good fits to two extreme outliers. We demonstrate that with SIDM the halo concentration, the baryon concentration and the back-reaction of baryons on the density profile play roles in explaining the rotation curves of these two extremes. SIDM halo profiles are flexible enough to accommodate the diverse rotation curves of spiral galaxies.

4 SUMMARY AND CONCLUSIONS

The SIDM model modifies the CDM paradigm by inclusion of non-gravitational interactions between dark matter particles in the halo evolution, and these self-interaction effects are most significant in the regions of halos with the high densities and velocity dispersions, i.e. within the scale radius of the halo. In the outer halo and at large scales SIDM is almost collisionless and retains the successes of ΛCDM . In the inner regions of halos the dark matter is redistributed into a central core, whose density and size depend on the microscopic particle interaction cross-section, the halo mass and even the baryon concentration. The mass profiles inferred from astronomical observations of the rotation curves of spiral galaxies thus offer an avenue to both constrain the self-interaction cross-section of dark matter and falsify or support specific self-interaction models.

Observationally, the shapes of the rotation curves of galaxies exhibit a wide diversity. We follow Oman et al. (2015) by

quantifying the range in the rotation curves using the relation between the total circular velocity measured within 2 kpc and at the peak, $V_{2\text{ kpc}}-V_{\text{max}}$. For a given V_{max} , the spread in $V_{2\text{ kpc}}$ can be a factor of four, which is difficult to reconcile in the prevailing Λ CDM paradigm (Oman et al. 2015), where dark matter is assumed to be collisionless over the cosmological timescale. This problem stems from the hierarchical structure formation in Λ CDM which produces a self-similar halo density profile, which is essentially parameterised by one parameter, the halo mass (or concentration). After we determine the halo mass by V_{max} , the halo circular velocity is completely fixed at all radii, up to the scatter, including the inner density cusp that is in contrast to the shallow (cored) one preferred by many dwarf galaxies. In addition, the enclosed mass of a CDM halo cusp tends to overwhelm the baryonic contribution and consequently also the scatter in $V_{2\text{ kpc}}$ caused by the spread in the baryon concentration. This inflexibility in CDM may be alleviated by introducing particular prescriptions of baryonic feedback processes that can dynamically heat the dark matter (Navarro et al. 1996; Pontzen & Governato 2012, and others), however SIDM offers an attractive alternative solution.

In this paper we have used controlled N-body simulations as a numerical experiment to test the SIDM model’s ability to address the diversity problem. We use the AREPO code to run isolated simulations of a live halo in the presence of a static baryonic disk in order to assess the gravitational impact of gas and stars on the halo evolution. This approach is suited to the SIDM model as dark matter self-interactions thermalise the inner halo and the final (inner) density profile is largely insensitive to the formation history. We sample a wide range of halo masses spanning about three orders of magnitude and vary the halo concentration within $\pm 2\sigma$ from its mean value. For each halo mass, we use abundance matching relations to choose the disk mass and we take three disk scale radii to span the baryon distributions. This sampling of the model parameter domain enables us to make concrete predictions of the rotation curves in the SIDM model.

Our main conclusion (see Fig. 3) is that the SIDM mechanism accommodates galaxies with a wide range of $V_{2\text{ kpc}}$ over the domain of V_{max} from 30–250 km s^{-1} . The spread in core densities is due in part to the variance in concentration (within $\pm 2\sigma$ from the mean), however this alone is insufficient to account for the large relative scatter of the observed values. Including self-interactions allows lower $V_{2\text{ kpc}}$, which requires low central densities in *both* baryons and dark matter. High values of $V_{2\text{ kpc}}$ are still achieved with compact baryonic disks where thermalisation into the deep baryonic potentials can induce NFW-like densities. As a result the predicted range of $V_{2\text{ kpc}}$ for a fixed V_{max} in SIDM is 50% larger than the CDM one, leading to a better agreement with the observed rotation curve distribution.

Some observed galaxies in the range $V_{\text{max}} = 60\text{--}80 \text{ km s}^{-1}$ and $V_{2\text{ kpc}} = 20\text{--}30 \text{ km s}^{-1}$ are still challenging. These cases might require assumptions about the structure of the copula of the combination of halo concentrations and baryonic disk sizes, in particular that very extended disks populate the most under-concentrated halos to reproduce the very low $V_{2\text{ kpc}}$, which is not an unrealistic assumption to first order. Nevertheless, the SIDM prediction is an improvement over CDM in all cases.

To further test our results, we have performed simulations to provide individual fits for two of the most extreme outliers highlighted in Oman et al. (2015), UGC 5721 and IC 2574, cusp- and core-dominated galaxies respectively, both with similar $V_{\text{max}} \approx 80 \text{ km s}^{-1}$ (see Figs. 5 and 6). Picking extreme $+0.9\sigma$ and -2.3σ concentrations from the halo concentration-mass relation, together

with a compact $R_d = 0.5 \text{ kpc}$ and extended $R_d = 3.0 \text{ kpc}$ baryonic distribution respectively, we find good fits in the SIDM paradigm. Interestingly, we find that the SIDM density profile can be as dense as the NFW one in a baryon-concentrated galaxy such as UGC 5721, because SIDM particles follow an isothermal distribution within the deep baryon potential. Our simulation result confirms the theoretical expectation first predicted in Kaplinghat et al. (2014). At the other extreme, IC 2574 with an inferred central dark matter dominated core is more straightforwardly tractable with a model that allows dark matter thermalisation, and is more challenging to the collisionless CDM model.

The implication of these elements is that with the inclusion of realistic baryonic components, SIDM models can produce quantitatively superior fits to rotation curves, both at the level of individual rotation curves and over the statistical distribution of a quantitative measure of their shapes. As one would expect, fitting the most extreme outliers requires an interplay between the combinations of halo concentration, the baryon distribution, and the influence of baryons on the SIDM halo profiles. The results from our numerical experiments fit well with the previous theoretical calculations of Kamada et al. (2016).

A number of avenues for future research are apparent. On the observational side, more detailed observations for mass modelling would allow tighter constraints on the dark matter distribution and consequently the interaction cross-section. Orthogonally, larger sample sizes would allow the $V_{2\text{ kpc}}-V_{\text{max}}$ distribution to better discriminate between CDM and SIDM. On the computational side, we have ignored the effects of the hierarchical assembly of dark matter halos. Whilst this is not expected to play a large role in the inner halo, it will nevertheless introduce additional scatter as a function of assembly time. Finally, all these will likely show strong correlations with the baryonic statistics, and investigations of galaxy formation in SIDM using full hydrodynamical cosmological simulations with the baryonic feedback processes are already being explored (e.g. Vogelsberger et al. 2014; Fry et al. 2015).

ACKNOWLEDGEMENTS

The authors would like to thank Andrew Pace for sharing his collocated data set for the rotation curves, Volker Springel for making AREPO available for this work and James Bullock, Simon White, Oliver Elbert, and Manoj Kaplinghat for useful discussions. This work was supported by the U.S. Department of Energy under Grant No. de-sc0008541 (HBY). HBY acknowledges support from the Hellman Fellows Fund. MV acknowledges support through an MIT RSC award and the support of the Alfred P. Sloan Foundation.

REFERENCES

- Behroozi P. S., Wechsler R. H., Conroy C., 2013, *ApJ*, **770**, 57
- Blais-Ouellette S., Amram P., Carignan C., 2001, *AJ*, **121**, 1952
- Blumenthal G. R., Faber S. M., Flores R., Primack J. R., 1986, *ApJ*, **301**, 27
- Boddy K. K., Feng J. L., Kaplinghat M., Tait T. M. P., 2014, *Phys. Rev. D*, **89**, 115017
- Boddy K. K., Kaplinghat M., Kwa A., Peter A. H. G., 2016, preprint, ([arXiv:1609.03592](https://arxiv.org/abs/1609.03592))
- Boylan-Kolchin M., Bullock J. S., Kaplinghat M., 2011, *MNRAS*, **415**, L40
- Brook C. B., 2015, *MNRAS*, **454**, 1719

- Brook C. B., Santos-Santos I., Stinson G., 2016, *MNRAS*, **459**, 638
- Buckley M. R., Fox P. J., 2010, *Phys. Rev.*, D81, 083522
- Côté S., Carignan C., Freeman K. C., 2000, *AJ*, **120**, 3027
- Cyr-Racine F.-Y., Sigurdson K., Zavala J., Bringmann T., Vogelsberger M., Pfrommer C., 2016, *Phys. Rev. D*, **93**, 123527
- Di Cintio A., Lelli F., 2016, *MNRAS*, **456**, L127
- Di Cintio A., Brook C. B., Dutton A. A., Macciò A. V., Stinson G. S., Knebe A., 2014, *MNRAS*, **441**, 2986
- Elbert O. D., Bullock J. S., Garrison-Kimmel S., Rocha M., Oñorbe J., Peter A. H. G., 2015, *MNRAS*, **453**, 29
- Elbert O. D., Bullock J. S., Kaplinghat M., Garrison-Kimmel S., Graus A. S., Rocha M., 2016, preprint, ([arXiv:1609.08626](https://arxiv.org/abs/1609.08626))
- Feng J. L., Kaplinghat M., Tu H., Yu H.-B., 2009, *J. Cosmology Astropart. Phys.*, **7**, 004
- Feng J. L., Kaplinghat M., Yu H.-B., 2010, *Physical Review Letters*, **104**, 151301
- Ferrero I., Abadi M. G., Navarro J. F., Sales L. V., Gurovich S., 2012, *MNRAS*, **425**, 2817
- Ferrero I., et al., 2017, *MNRAS*, **464**, 4736
- Firmani C., D’Onghia E., Avila-Reese V., Chincarini G., Hernández X., 2000, *MNRAS*, **315**, L29
- Flores R. A., Primack J. R., 1994, *ApJ*, **427**, L1
- Fry A. B., et al., 2015, *MNRAS*, **452**, 1468
- Garrison-Kimmel S., Rocha M., Boylan-Kolchin M., Bullock J. S., Lally J., 2013, *MNRAS*, **433**, 3539
- Gnedin O. Y., Ostriker J. P., 2001, *ApJ*, **561**, 61
- Governato F., et al., 2010, *Nature*, **463**, 203
- Hayashi E., et al., 2004, *MNRAS*, **355**, 794
- Hernquist L., 1990, *ApJ*, **356**, 359
- Hernquist L., 1993, *ApJS*, **86**, 389
- Huang S., Haynes M. P., Giovanelli R., Brinchmann J., 2012, *ApJ*, **756**, 113
- Kahlhoefer F., Schmidt-Hoberg K., Frandsen M. T., Sarkar S., 2014, *MNRAS*, **437**, 2865
- Kamada A., Kaplinghat M., Pace A. B., Yu H.-B., 2016, preprint, ([arXiv:1611.02716](https://arxiv.org/abs/1611.02716))
- Kaplinghat M., Keeley R. E., Linden T., Yu H.-B., 2014, *Physical Review Letters*, **113**, 021302
- Kaplinghat M., Tulin S., Yu H.-B., 2016, *Physical Review Letters*, **116**, 041302
- Katz H., Lelli F., McGaugh S. S., Di Cintio A., Brook C. B., Schombert J. M., 2017, *MNRAS*, **466**, 1648
- Kim S. Y., Peter A. H. G., Wittman D., 2016, preprint, ([arXiv:1608.08630](https://arxiv.org/abs/1608.08630))
- Kuzio de Naray R., McGaugh S. S., de Blok W. J. G., 2008, *ApJ*, **676**, 920
- Kuzio de Naray R., Martinez G. D., Bullock J. S., Kaplinghat M., 2010, *ApJ*, **710**, L161
- Loeb A., Weiner N., 2011, *Physical Review Letters*, **106**, 171302
- Ludlow A. D., Navarro J. F., Angulo R. E., Boylan-Kolchin M., Springel V., Frenk C., White S. D. M., 2014, *MNRAS*, **441**, 378
- McCarthy I. G., Schaye J., Font A. S., Theuns T., Frenk C. S., Crain R. A., Dalla Vecchia C., 2012, *MNRAS*, **427**, 379
- Miralda-Escudé J., 2002, *ApJ*, **564**, 60
- Miyamoto M., Nagai R., 1975, *PASJ*, **27**, 533
- Moore B., 1994, *Nature*, **370**, 629
- Navarro J. F., Eke V. R., Frenk C. S., 1996, *MNRAS*, **283**, L72
- Navarro J. F., Frenk C. S., White S. D. M., 1997, *ApJ*, **490**, 493
- Oñorbe J., Boylan-Kolchin M., Bullock J. S., Hopkins P. F., Kereš D., Faucher-Giguère C.-A., Quataert E., Murray N., 2015, *MNRAS*, **454**, 2092
- Oh S.-H., de Blok W. J. G., Brinks E., Walter F., Kennicutt Jr. R. C., 2011, *AJ*, **141**, 193
- Oh S.-H., et al., 2015, *AJ*, **149**, 180
- Oman K. A., et al., 2015, *MNRAS*, **452**, 3650
- Pace A. B., 2016, preprint, ([arXiv:1605.05326](https://arxiv.org/abs/1605.05326))
- Papastergis E., Shankar F., 2016, *A&A*, **591**, A58
- Papastergis E., Giovanelli R., Haynes M. P., Shankar F., 2015, *A&A*, **574**, A113
- Persic M., Salucci P., Stel F., 1996, *MNRAS*, **281**, 27
- Peter A. H. G., Rocha M., Bullock J. S., Kaplinghat M., 2013, *MNRAS*, **430**, 105
- Pineda J. C. B., Hayward C. C., Springel V., Mendes de Oliveira C., 2017, *MNRAS*, **466**, 63
- Planck Collaboration et al., 2014, *A&A*, **571**, A16
- Pontzen A., Governato F., 2012, *MNRAS*, **421**, 3464
- Randall S. W., Markevitch M., Clowe D., Gonzalez A. H., Bradač M., 2008, *ApJ*, **679**, 1173
- Read J. I., Agertz O., Collins M. L. M., 2016a, *MNRAS*, **459**, 2573
- Read J. I., Iorio G., Agertz O., Fraternali F., 2016b, *MNRAS*, **462**, 3628
- Rhee G., Valenzuela O., Klypin A., Holtzman J., Moorthy B., 2004, *ApJ*, **617**, 1059
- Robertson A., Massey R., Eke V., 2017, *MNRAS*, **465**, 569
- Rocha M., Peter A. H. G., Bullock J. S., Kaplinghat M., Garrison-Kimmel S., Oñorbe J., Moustakas L. A., 2013, *MNRAS*, **430**, 81
- Sales L. V., et al., 2017, *MNRAS*, **464**, 2419
- Sanders R. H., McGaugh S. S., 2002, *ARA&A*, **40**, 263
- Santos-Santos I. M., Brook C. B., Stinson G., Di Cintio A., Wadsley J., Domínguez-Tenreiro R., Gottlöber S., Yepes G., 2016, *MNRAS*, **455**, 476
- Sawala T., et al., 2015, *MNRAS*, **448**, 2941
- Schaller M., et al., 2015, *MNRAS*, **451**, 1247
- Schneider A., Trujillo-Gomez S., Papastergis E., Reed D. S., Lake G., 2016, preprint, ([arXiv:1611.09362](https://arxiv.org/abs/1611.09362))
- Shen S., Mo H. J., White S. D. M., Blanton M. R., Kauffmann G., Voges W., Brinkmann J., Csabai I., 2003, *MNRAS*, **343**, 978
- Spekkens K., Giovanelli R., Haynes M. P., 2005, *AJ*, **129**, 2119
- Spergel D. N., Steinhardt P. J., 2000, *Physical Review Letters*, **84**, 3760
- Springel V., 2010, *MNRAS*, **401**, 791
- Springel V., Di Matteo T., Hernquist L., 2005, *MNRAS*, **361**, 776
- Swaters R. A., Madore B. F., van den Bosch F. C., Balcells M., 2003, *ApJ*, **583**, 732
- Swaters R. A., Sanders R. H., McGaugh S. S., 2010, *ApJ*, **718**, 380
- Tollet E., et al., 2016, *MNRAS*, **456**, 3542
- Tulin S., Yu H.-B., Zurek K. M., 2013a, *Phys. Rev. D*, **87**, 115007
- Tulin S., Yu H.-B., Zurek K. M., 2013b, *Physical Review Letters*, **110**, 111301
- Tully R. B., Fisher J. R., 1977, *A&A*, **54**, 661
- Vogelsberger M., Zavala J., Loeb A., 2012, *MNRAS*, **423**, 3740
- Vogelsberger M., Zavala J., Simpson C., Jenkins A., 2014, *MNRAS*, **444**, 3684
- Vogelsberger M., Zavala J., Cyr-Racine F.-Y., Pfrommer C., Bringmann T., Sigurdson K., 2016, *MNRAS*, **460**, 1399
- Wetzel A. R., Hopkins P. F., Kim J.-h., Faucher-Giguère C.-A., Kereš D., Quataert E., 2016, *ApJ*, **827**, L23

Yoshida N., Springel V., White S. D. M., Tormen G., 2000, *ApJ*, **544**, L87

Zavala J., Vogelsberger M., Walker M. G., 2013, *MNRAS*, **431**, L20

de Blok W. J. G., McGaugh S. S., Rubin V. C., 2001, *AJ*, **122**, 2396

de Blok W. J. G., Walter F., Brinks E., Trachternach C., Oh S.-H., Kennicutt Jr. R. C., 2008, *AJ*, **136**, 2648

van den Bosch F. C., Robertson B. E., Dalcanton J. J., de Blok W. J. G., 2000, *AJ*, **119**, 1579

APPENDIX A: JEANS ANALYSIS

In order to accelerate the analysis of the spherically symmetric cases we have employed ‘Jeans analysis’ (Kaplinghat et al. 2016) which gives a very good approximation to the final density distribution of halo-like systems. For the benefit of the astrophysics reader we discuss the self-similar evolution of the dark matter only case here, for more complex cases one should consult the aforementioned reference.

For the spherically-symmetric dark matter only case, the distribution function of dark matter can be written as $f(r, v_{\parallel}, v_{\perp})$ with density $\rho_{\text{ini}}(r)$. An approximation to the effects of self-interaction, referred to as Jeans analysis, is to assume that those regions of the halo with $\lesssim 1$ scattering over the evolution are unperturbed, whilst those with $\gtrsim 1$ have become fully collisional (i.e. act as an ideal gas) and isothermal (i.e. erased any thermal gradient). Whilst this approximation may seem relatively severe, one should recall that a dark matter halo encompasses many orders of magnitude in density and velocity dispersion, and so the majority of the volume is either highly collisional or nearly collisionless. Finding the radius r_1 at which approximately 1 scattering per evolution time T occurs is determined implicitly via

$$\frac{\langle \sigma_{\text{T}} v \rangle}{m_{\chi}} \rho_{\text{ini}}(r_1) T = 1, \quad (\text{A1})$$

and subsequently the evolved profile (assuming f_{ini} was a stationary state) is the piecewise solution

$$\rho(r) = \begin{cases} \rho_{\text{iso}}(r) & r < r_1 \\ \rho_{\text{ini}}(r) & r \geq r_1 \end{cases} \quad (\text{A2})$$

where $\rho_{\text{iso}}(r)$ is the isothermal solution to the Jeans equation (see below) with $\rho_{\text{iso}} \rightarrow$ a constant as $r \rightarrow 0$ that matches the density and mass enclosed ρ_1 and M_1 at r_1 .

A0.1 Solution for ρ_{iso}

Consider Poisson’s equation for an isothermal self gravitating spherically symmetric halo

$$\sigma_0^2 \nabla^2 \ln \rho = -4\pi G \rho \quad (\text{A3})$$

As a second order differential equation this has 2 unknowns, which extends to a third if we consider σ_0 (the velocity dispersion) to be unknown. If we know two values, e.g. ρ_1 and M_1 at some radius r_1 , then we need an additional constraint, but this can be provided by choosing the ‘cored’ solution with $\rho \rightarrow$ a constant as $r \rightarrow 0$.

Denoting this constant ρ_c a good choice for similarity function turns out to be for the ratio of the mean enclosed density $\bar{\rho}$ to this, i.e. $\theta = \frac{\bar{\rho}}{\rho_c}$. Expanding the Taylor series about $r = 0$ tells us the leading order non-constant term is $O(r^2)$, i.e. w.l.o.g we can write

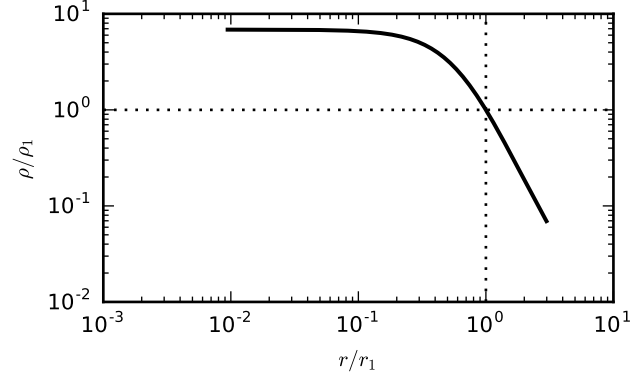
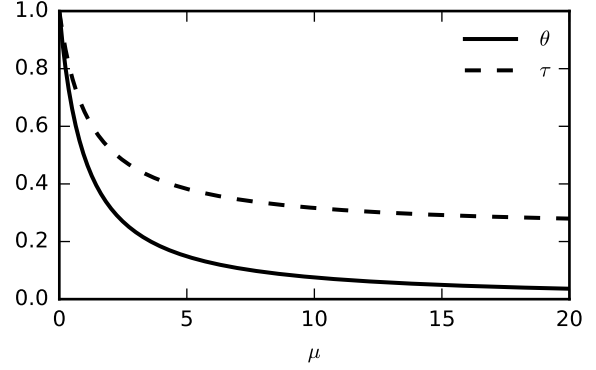


Figure A1. Upper panel: $\theta(\mu)$ and $\tau(\mu)$ functions. Lower panel, example Jeans solution for $\tau_1 = \frac{1}{2}$, i.e. at r_1 the density is half the mean density

$\theta \sim 1 - \frac{r^2}{r_c^2}$ (for some core size r_c) as $r \rightarrow 0$. This suggests the use of the dimensionless variable

$$\mu = \frac{r^2}{r_c^2}, \quad (\text{A4})$$

as a parameter for $\theta(\mu)$, and by substitution

$$\theta(0) = -\theta'(0) = 1 \quad (\text{A5})$$

where the prime denotes differentiation w.r.t. μ , and we have chosen r_c to satisfy

$$\sigma_0^2 = \frac{2\pi}{5} G r_c^2 \rho_c. \quad (\text{A6})$$

By substitution into Eqn. (A3) we determine that $\theta(\mu)$ obeys the 2nd order nonlinear ODE

$$\theta = -\frac{3}{5} \frac{d}{d\mu} \ln(3\theta + 2\mu\theta'). \quad (\text{A7})$$

We plot this function in the left panel of Fig. A1. In order to determine the density we may wish to tabulate θ along with the dimensionless density ratio function we will refer to as τ , determined from θ by

$$\tau(\mu) = \frac{\rho}{\bar{\rho}} = 1 + \frac{2\mu\theta'}{3\theta}. \quad (\text{A8})$$

which is monotonically decreasing.

Given some point r_1 at which we know the density ρ_1 and the mass enclosed M_1 , then we know the mean density and can simply read off the μ_1 that gives us this τ_1 , i.e.

$$\tau(\mu_1) = \tau_1 = \frac{4\pi r_1^3 \rho_1}{3M_1} \quad (\text{A9})$$

and then substitute to find the density at any $r < r_1$, i.e.

$$\rho_{\text{iso}}(r) = \bar{\rho}\tau = \rho_1 \frac{\tau \left(\frac{\mu_1 r^2}{r_1^2} \right) \theta \left(\frac{\mu_1 r^2}{r_1^2} \right)}{\tau_1 \theta_1}. \quad (\text{A10})$$

and we plot an example in the right panel of Fig. A1

A0.2 Scale dependence

Since the halos in cosmological simulations are self-similar, the features are broadly speaking common to all halo masses. In particular in Eqn. (A1), for a fixed halo concentration (at all halo masses) the density $\rho_{\text{ini}}(r/r_{200})$ is fixed, and so the scale dependent differences occur due to the increasing velocity dispersions and falling concentrations of larger halos. Increasing velocity dispersion increases the scattering rate and causes core formation to progress faster, whilst lower concentrations reduce the central densities, and consequently the scattering rate and core formation. Overall the velocity dispersion effect dominates and larger halos tend to grow their cores faster, up to some limit where velocity dependent cross-sections become important, although we do not discuss that case here.

APPENDIX B: NFW VS. HERNQUIST ICS

As mentioned in Section 2.2, the NFW and Hernquist initial conditions can evolve slightly differently in SIDM, driven by their velocity dispersion profiles (the NFW profile has somewhat increased velocity dispersion just beyond the scale radius r_s). In particular once the radius of unit scattering r_1 has saturated r_s , the Hernquist halo has slightly less ‘heat’ (i.e. velocity dispersion) for SIDM to transfer than NFW. Since halos in cosmological N-body simulations have profiles closer to NFW than to Hernquist, we wish to test whether there are systematic differences due to the use of Hernquist halos for our SIDM simulations.

In order to test this, we performed simulations similar to those of the IC 2574 and UGC 5721 cases (although not actually our final best-fits given in Table 2). We created NFW halos using the publicly available SPHERIC⁴ code (Garrison-Kimmel et al. 2013) and equivalent Hernquist halos matched via Eqn. (3). Notably the mass distributions are not the same outside the scale radius r_s even in the ICs, so we do not expect perfect fits even ignoring the differences in velocity dispersion profiles. In Fig. B1 we have plotted the profiles after 10 Gyr of evolution with $\sigma_T/m_\chi = 3 \text{ cm}^2 \text{ g}^{-1}$ with the dark matter contribution and the total rotation curves implied by a realistic baryonic contribution. One can see that for the low concentration halo (upper panel), the differences are truly negligible. On the other hand, for the higher concentration halo (lower panel, very similar to the $+0.9\sigma$ of UGC 5721), the extra velocity dispersion (and consequently larger core radius) of the evolved NFW case becomes apparent, albeit only at the level of $\approx 10\%$. From this we infer that the central densities from high concentration halos are overestimated with the Hernquist model, and if one wishes to use equivalent NFW halos one should increase the concentration (use a shorter r_s) by a few percentage points, including those parameters in Section 3.3.

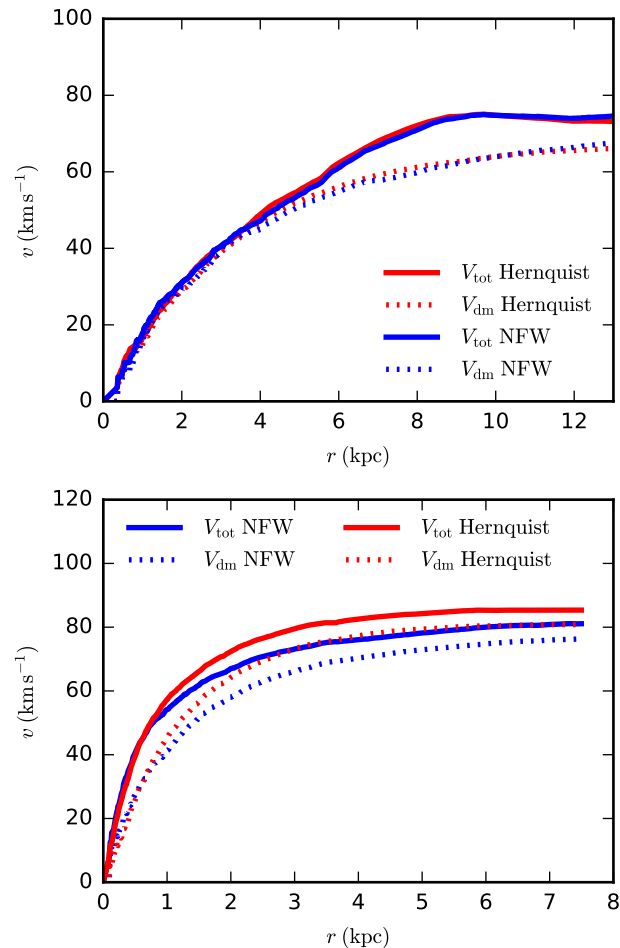


Figure B1. Comparison of the evolution of ‘equivalent’ Hernquist and NFW halos in the presence of baryonic disks. *Upper panel* is a low concentration halo very similar to our IC 2574 fit, whilst *lower panel* is high concentration setup similar to that of UGC 5721. The total rotation curves for the Hernquist halo are shown in *solid red* vs. the NFW in *solid blue*, with the dark matter contributions in *dotted lines* respectively.

⁴ <https://bitbucket.org/migroch/spheric>